Constant-pressure molecular-dynamics simulations of the crystal-smectic transition in systems of soft parallel spherocylinders

K. M. Aoki and F. Yonezawa
Department of Physics, Faculty of Science and Technology, Keio University, 3-14-1 Hiyoshi, Kohoku-ku, Yokohama 223, Japan

(Received 16 April 1992; revised manuscript received 8 July 1992)

In order to investigate thermodynamic properties and microscopic structure around the crystal-smectic transition, we present constant-pressure molecular-dynamics simulations for soft parallel spherocylinders as a model for liquid crystals. The method of Andersen [J. Chem. Phys. **72**, 2384 (1980)] as well as the method of Parrinello and Rahman [Phys. Rev. Lett. **45**, 1196 (1980)] are applied to a right parallelepiped simulation box, and the equation of state for this model is evaluated. Thermodynamic properties such as enthalpy and volume as functions of reduced density ρ^* or of temperature show a clear first-order transition. The dependence of $l_\perp$, the square root of the specific area of the plane perpendicular to the molecular axis, on ρ^* shows a feature characteristic of two-dimensional melting. We calculate the specific length l_z in the direction of the molecular axis, which corresponds to the thickness of a smectic layer in the liquid-crystal region. From the ρ^* dependence of l_z and $l_z/l_\perp$, we show that the anisotropy of the molecular volume plays an important role in the crystal-smectic transition. We also observe a clear change in both diffusion and structural properties before and after this transition. The mean-square displacements in directions perpendicular to the alignment show that in the smectic phase the molecules diffuse freely within the layers, although the density wave in the direction perpendicular to layers does exist even after the transition.

PACS number(s): 61.30.−v, 64.70.Md

I. INTRODUCTION

Liquid crystals are intermediate states of aggregation of organic compounds between crystalline solid and isotropic liquid. They are characterized by molecular orientational order. In particular, the nematic phase has orientational order alone, while other liquid-crystal phases have some additional kinds of order. Altogether up to 17 different thermotropic liquid-crystal phases have been identified [1].

In this paper, we confine our interest to smectic-liquid-crystal phases. They are composed of molecules segregating into periodic layers. In other words, the time average of the molecular position forms a one-dimensional density wave. In this phase, the layers are able to slide over one another relatively easily. The simplest smectic phase is the smectic A phase in which the average of the molecular long axis is perpendicular to the layers. When the molecular director makes an angle other than 90° to the layers, the phase is called smectic C. In both smectic A and C phases, each layer is liquidlike in the sense that the molecules diffuse separately in each layer. On the other hand, the smectic B (hexatic B) phase has a long-range sixfold bond orientational order in addition to the layer structure.

Many attempts have been made to understand these complex fluids. As early as in the 1940s, Onsager developed a theory which takes the excluded volume effect into account, and he pointed out that the orientational ordering in nematic-liquid-crystal phases can occur in a system with repulsive forces alone [2]. Since the late 1950s, many models with attractive forces have been proposed. Although some of these models are rather empirical, they can explain the behavior of both nematic and smectic phases. On the basis of these studies it was widely believed that the attractive force is indispensable for the appearance of smectic phases. In 1979 Hosino, Nakano, and Kimura calculated the free energy of hard-rod systems within the second and third virial approximation and predicted the existence of a smectic phase even in a system without attractive force [3].

Molecular-dynamics (MD) computer simulations are now an established method for analyzing microscopic structures and have the advantage over other theoretical approaches, such as mean-field approximations, that the MD techniques do not involve any uncontrollable approximations once the interactions among the molecules are given. The MD simulations have an advantage over Monte Carlo (MC) simulations in the sense that they treat the time evolution of the molecular motions directly so that we are able to obtain diffusion processes.

For a system composed of hard spheres, the seminal MD simulations by Alder and Wainwright showed that the solid-fluid first-order transition will occur in a system with repulsive force alone [4]. The early MD simulations of anisotropic particles of Robertus and Sando did not show any liquid-crystal phase for hard spherocylinders [5]. In 1987, Stroobants, Lekkerkerker, and Frenkel studied a system of parallel spherocylinders by MC simulations and ascertained that a smectic phase can also be formed by hard-core repulsion [6]. In 1990, Veerman and Frenkel extended this work to a system of hard

spherocylinders with full orientational freedom and carried out constant volume MD simulations after preparing well-equilibrated configurations by MC simulations and observed stable nematic and smectic phases [7]. This work shows that the introduction of orientational freedom increases the anisotropy necessary to exhibit a smectic phase when compared to the system with molecules constrained to be parallel to each other.

For soft-core spheres, solid-fluid phase-transition densities have been determined numerically for different values of the exponent n in the soft-core potential by MC simulations [8]. The dependence of physical properties on the inverse power n are also calculated including hard spheres as $n = \infty$. For instance, the reduced melting densities ρ^* are larger when n is smaller (potentials are softer). On the other hand, systems of anisotropic molecules with soft-core repulsion have not been studied by MD simulations to our knowledge.

Although real liquid crystals have potentials that include both the repulsive and attractive forces, it is very interesting to determine the role of each force. Here we confine our interest to repulsive interactions and study systems of parallel spherocylinders described by an inverse-power pair potential. Another point to make is that this is an attempt at constant-pressure MD simulations for systems of anisotropic particles. In this paper, we report on the thermodynamic properties of the crystalline-solid to smectic-liquid-crystal transition. We also analyze the differences between the crystalline and smectic phases to see whether these smectics, realized by repulsive force alone, possess the characteristics observed in real smectic liquid crystals.

In Sec. II, the model and methods are explained. In Sec. III the results are discussed in two divided subsections; Sec. III A discusses thermodynamic properties and Sec. III B gives a diffusion and structural analysis. Concluding remarks are given in Sec. IV.

II. MODEL AND METHODS

A. Model

We study a model of soft-core parallel spherocylinders (cylinders with length L and diameter D, capped at each end with hemispheres of the same diameter). The long axes of the molecules are fixed to the z axis of the MD simulation box. We use a potential defined by

$$\phi(r_{ij}) = \varepsilon \left(\frac{D}{r_{ij}}\right)^n , \tag{1}$$

where

$$r_{ij}^2 = \begin{cases} x_{ij}^2 + y_{ij}^2, & -L < z_{ij} < L \\ x_{ij}^2 + y_{ij}^2 + (z_{ij} - L)^2, & \text{otherwise,} \end{cases}$$

where r_{ij} is the distance between the ith and jth molecule, i.e., $r_{ij} = |\mathbf{r}_{ij}| = |\mathbf{r}_j - \mathbf{r}_i|$, $\mathbf{r}_i$ and $\mathbf{r}_j$ being, respectively, the positional vectors of the ith and jth molecule; x_{ij}, y_{ij}, and z_{ij} are respectively the x, y, and z components of $\mathbf{r}_{ij}$. We choose the inverse power n to be 14 which corresponds to a relatively fast decay. We take the unit of energy as ε and the unit of length as D.

In this work, we keep the ratio of the length and the diameter of the cylinder L/D fixed at unity so that the anisotropy of the molecule ($\frac{L}{D} + 1$) is 2.

B. Methods

1. General aspects

In order to investigate the thermodynamic properties and microscopic structure, we perform constant-pressure MD simulations in several ways.

It is known that the scaling property exists for systems of soft-core potentials and the equation of state can be expressed uniquely in terms of the reduced density ρ^*. The reduced density we use is defined as $\rho^* = Nv_0/VT^{3/n}$, where N is the total number of molecules, V is the total volume of the system, and T is the temperature. We introduce $v_0 = \frac{1}{6}\pi D^3(1 + \frac{3}{2}\frac{L}{D})$ which can be defined as the volume of a molecule because it is convenient to compare data for systems of different anisotropies. We verified that the scaling property is well preserved even for a small system size $N = 108$ of soft-core spheres ($L/D = 0$) by both constant-volume and constant-pressure MD simulations.

For each simulation the temperature is kept constant by the constraint method and periodic boundary conditions are applied. Different system sizes are examined to observe the system-size effects and different initial configurations are employed to make sure that the results do not depend on them. The long axis of the spherocylinders are fixed to the z direction of the MD box. In each simulation we start with an initial configuration in which the molecules are arranged as stacks of two-dimensional triangular lattices in the xy plane. The main results we report here are for a number of molecules N and an initial configuration as shown in Table I. The time step Δt for integration is chosen to be $\Delta t = 2.0 \times 10^{-4}$ in units of $(mD^2/\varepsilon)^{\frac{1}{2}}$, where m is the mass of the molecule. This value of Δt is smaller than one-hundredth of the period in the velocity correlation function.

2. Constant-pressure simulations

Initially, for the purpose of getting a picture of the overall behavior, we used Andersen's constant-pressure method in a cubic MD box [9]. We found that, for a cubic cell, there is an imbalance of the internal stress tensor between the z direction and the xy direction. Since this situation does not simulate the actual environment under the hydrostatic pressure, we adopt several other methods

TABLE I. System sizes and initial configurations.

	Initial configuration	
Number of molecules	Number of layers	Type of stacking
224	4	*ABAB*
600	5	*AAAAA*
792	6	*ABCABC*

as described below.

For the crystalline-solid phase, the method of constant pressure by Parrinello and Rahman [10] is applied in a restricted manner that only the length of the MD box can change but not the angles [11]. For our simulation box, we chose a right parallelepiped so that the edge length L_x in the x direction is equal to L_y, the length in the y direction, and we write $L_\perp \equiv L_x = L_y$. In this model, only the diagonal elements of the internal stress tensor $\mathbf{\Pi}$ are nonzero. In addition, the requirement $L_x = L_y$ leads to the condition $\Pi_{xx} = \Pi_{yy} \equiv P_\perp$. This quantity is interpreted as the pressure acting on the four side walls, which surround the parallel spherocylinders, of the simulation box. On the other hand, $\Pi_{zz} \equiv P_z$ is the pressure acting on the upper and lower walls of the box.

In the conventional Parrinello and Rahman method, the shape and volume of the simulation box change automatically according to the change in the instantaneous pressure. Therefore the method is most appropriate in the study of crystalline-structure phase transitions. When we apply this method to our system of parallel spherocylinders, the molecules start diffusing when the temperature (or reduced density) reaches a certain value and we can specify that value as the melting temperature (or melting density). Above this temperature (or below this density), it turns out that the system becomes a one-layer structure because of the fluctuation perpendicular to the layers. This suggests that the automatic shape and volume change in the Parrinello and Rahman method is too sensitive for a system in which the constituent particles diffuse. In order to avoid this problem, we use the following three methods for the liquid-crystal phase.

(i) We modify Andersen's method in such a way that the edge length L_z in the direction of the molecular axis is not necessarily identical to $L_\perp$, but the ratio $L_z/L_\perp$ is kept constant during each run.

(ii) We apply a further restriction that L_z =const to the Parrinello and Rahman method of a right parallelepiped simulation box. In this way the four walls of the MD box in the directions of the molecular short axis are allowed to fluctuate depending on the internal pressure and will relax to equilibrium.

(iii) We fix the value of $L_\perp$ in contrast to the upper method, so that only the two walls in the long direction of the molecules can vary.

The fundamental outline of these three methods is better understood by referring to Table II where $P_{\rm ex}$ denotes the desired external pressure. The quantity to be fixed during each simulation is given in the first column. The relation in the second column is guaranteed from the requirement of each constant-pressure method itself. What we have to do is actually search the density (or temperature) that gives the condition presented in the third column where the angular brackets denote the average over a certain duration of time steps. We adopt only those data that satisfy the condition in the third column within 5% error.

Every run consists of more than 5000 time steps and all values reported here are the averages over the last 1000 time steps of each run.

III. RESULTS

The results reported in this paper are obtained from the appropriate constant-pressure simulation methods mentioned in the previous section. The method of Parrinello and Rahman is applied for the crystalline-solid phase, and for the liquid-crystal phase we apply all three methods explained in Table II. We divide this section into two parts. In Sec. III A, we mainly report on the thermodynamic properties. Section III B is dedicated to the diffusion properties and structural analysis where we discuss the crystal-solid and liquid-crystal phases separately.

A. Thermodynamic properties

Combining the data of all the methods we get a graph of the equation of state (Fig. 1). Data for both system sizes $N = 600$ and $N = 244$ are plotted in this graph. Each symbol specifies both the method and the system size as indicated in Table III unless it is stated otherwise. We observe a clear first-order transition in this equation of state. We show in Sec. III B that the state after melting is ascertained to be the smectic-liquid-crystal phase from the behaviors of the mean-square displacements and the pair-distribution functions. Note that in all the figures in this section we show the data for two sizes as denoted in Table III. As will be seen, the size effect turns out to be small.

Enthalpy per particle is defined $H/N = (PV+U_{\rm int})/N$ where P is the pressure, V is the volume, $U_{\rm int}$ the internal energy, and N the number of particles. At the density where the transition takes place in the equation of state, we observe a discontinuous change in H/N as seen in Fig. 2. We propose two explanations for why the deviations are relatively large in the liquid-crystal density region: (1) this quantity H includes errors of three thermodynamic quantities P, V, and $U_{\rm int}$. (2) This quantity H is rather sensitive to the method employed.

The specific volume V/N as a function of temperature

TABLE II. Explanations of our constant-pressure MD methods for simulating liquid crystals.

Method	Fixed value	Automatically satisfied in each method	The correlation we have to search by changing ρ^* or T
(i)	$L_z/L_\perp$	$2\langle P_\perp\rangle + \langle P_z\rangle = P_{\rm ex}$	$\langle P_\perp\rangle \simeq \frac{1}{3}P_{\rm ex}$, $\langle P_z\rangle \simeq \frac{1}{3}P_{\rm ex}$
(ii)	L_z	$\langle P_\perp\rangle = \frac{1}{3}P_{\rm ex}$	$\langle P_z\rangle \simeq \frac{1}{3}P_{\rm ex}$
(iii)	$L_\perp$	$\langle P_z\rangle = \frac{1}{3}P_{\rm ex}$	$\langle P_\perp\rangle \simeq \frac{1}{3}P_{\rm ex}$

TABLE III. Symbols in figures.

Region	Simulation method	System size $N = 600$	System size $N = 224$
Crystal	Parrinello and Rahman	●	×
Liquid	Method (i)	◇	□
crystal	Method (ii)	△	+
	Method (iii)	○	▽

T is given in Fig. 3(a) for $N = 224$ and in Fig. 3(b) for $N = 600$. In Fig. 3(a), we use the symbols defined in the third column of Table III instead of the fourth column. In both figures, the temperature is described in units such that $T = 500$ for $\rho^* = 0.50$. The data is nearly linear in the crystal phase as well as in the smectic phase. There exists a steep change between the two phases. The error bars for system size $N = 600$ are much smaller than those for $N = 224$ especially after the transition. This clearly shows that the fluctuation is smaller for larger system size.

In order to study the microscopic situation around the transition, it is interesting to see the anisotropy of the specific volume v_m associated with each molecule. We define the specific volume v_m such that $v_m \equiv V/N = l_z l_\perp^2$ where $l_z = L_z/n_z$, n_z being the number of layers, and $l_\perp = (L_\perp^2/n_\perp)^{\frac{1}{2}}$, $n_\perp$ being N/n_z. The ratio $l_z/l_\perp$ serves as a measure for the anisotropy of the specific volume or of the space required for each molecule. From Fig. 4, we see that in the region we study, the anisotropy of the specific volume $l_z/l_\perp$ is larger than the anisotropy of the molecule ($\frac{L}{D} + 1 = 2$). A discontinuous change is observed in $l_z/l_\perp$ at the transition density region.

It is also interesting to study the density dependence of $l_\perp$ and l_z as shown in Figs. 5 and 6, respectively. In the crystal region, $l_\perp$ increases continuously while l_z is almost constant except for the pretransition region. At the transition density, a discontinuous change is observed in $l_\perp$, indicating that two-dimensional melting takes place in the direction perpendicular to the molecular axis. As

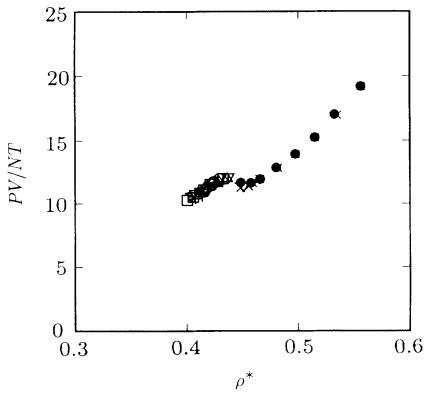

FIG. 1. Equation of state of parallel spherocylinders of anisotropy $\frac{L}{D} + 1 = 2$, calculated from four different constant-pressure MD methods.

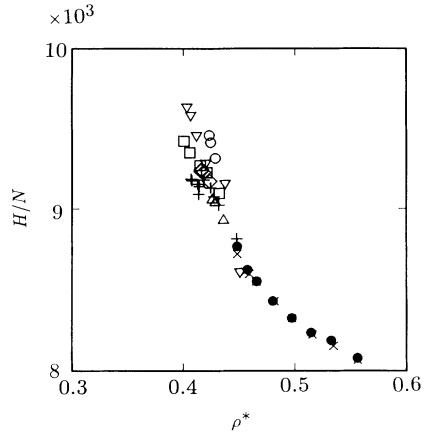

FIG. 2. Enthalpy per particle H/N plotted against reduced density ρ^*.

we show in Sec. III B, the molecules actually diffuse along the layers. On the other hand, l_z decreases in the transition region. The decrease is considered to come from the fact that the volume expansion on melting in the direction of layers makes it easier for the spherocylinder caps of the molecules to be pushed into each other's adjacent layers.

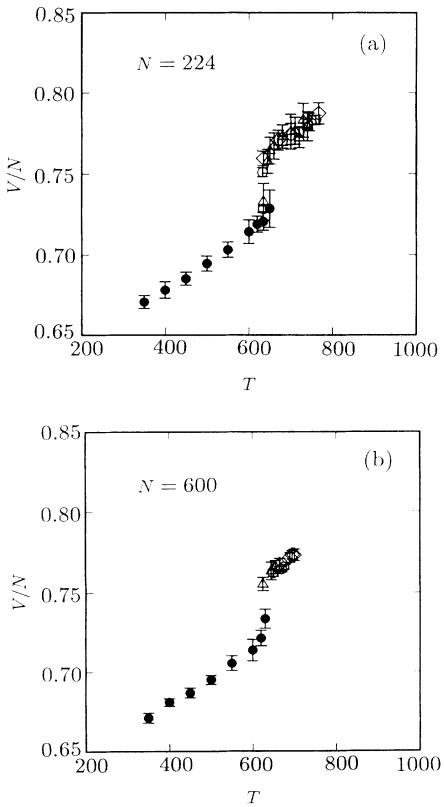

FIG. 3. Specific volume V/N as a function of temperature T for system size (a) $N = 224$ and (b) $N = 600$. For both systems ● denotes values from the method of Parrinello and Rahman; ◇ denotes data from method (i); △, method (ii); and ○, method (iii).

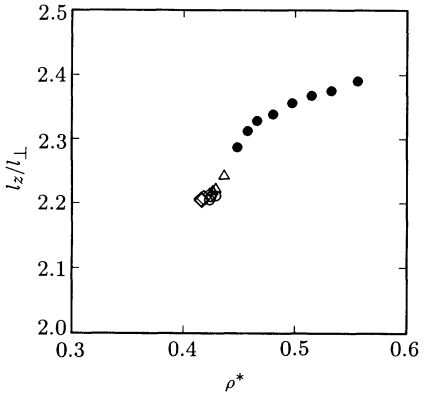

FIG. 4. Ratio of molecular lengths $l_z/l_\perp$ vs reduced density ρ^* for $N = 600$.

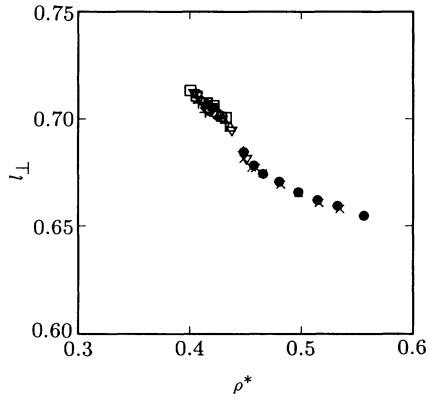

FIG. 5. Molecular length perpendicular to the long axis $l_\perp$ as a function of reduced density ρ^*.

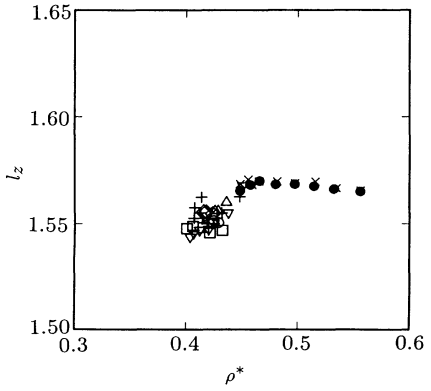

FIG. 6. Molecular length parallel to the long axis l_z as a function of reduced density ρ^*.

These results mentioned above show that the shape of the MD simulation box should not be fixed for simulating anisotropic molecules.

B. Diffusion and structural analysis.

In this subsection, we show the results for diffusion and structure for two different densities separately, one higher and another lower than the density at the crystal-smectic transition observed by thermodynamic properties. The main properties observed are the mean-square displacement in each direction to analyze the diffusion processes and the correlation functions in direction parallel and perpendicular to the molecular axis by computing the average pair-distribution function. We also show the average molecular positions.

1. Crystalline-solid phase

We start our constant-pressure MD simulations in the crystalline-solid phase from six different initial configurations for system sizes $N = 224$ (four layers), $N = 600$ (five layers), and $N = 792$ (six layers), and we obtain structures as presented in Table IV. The characteristic feature common to all these six structures is that the layers are stacked in the close-packed configuration where the molecules in adjacent layers never stack on top of one another. It is also obvious from Table IV that the order of stacking does not extend beyond the nearest-neighbor layers. It is interesting to note that when the energies of close-packed structures are compared at absolute zero for a system of Lennard-Jones spheres, the differences in the minimum potential energies among an hcp ($ABAB$), a random stacking, and an fcc ($ABCABC$) are negligibly small (less than 0.01%). So it is not surprising that the system does not show much preference for a particular stacking.

In what follows, we present diffusion and structural analysis results for a system with number of molecules $N = 600$. For the crystalline-solid phase we show the results for $\rho^* = 0.534$.

For the case in which we start from the stacking $AAAAA$, the mean-square displacement (MSD) in the direction parallel to the molecular axis z (the broken curve) and perpendicular to it (the solid curve, x direc-

TABLE IV. Initial configurations and resulting structures in the crystalline-solid phase.

Initial configuration		Resulting structure
Number of layers	Type of stacking	Type of stacking
4	$ABAB$	$ABAB$
	$AAAA$	$ABAB$
5	$AAAAA$	$ABCAB$
6	$ABCABC$	$ABCABC$
	$ABABAB$	$ABABAB$
	$AAAAAA$	$ABCBAB$

tion; the dashed curve, y direction) are shown in Fig. 7. The MSD's are given in units of D^2 since the distances are measured in unit D throughout this article. It is seen from the figure that the molecules do not stay in the initial configuration of $AAAAA$ but rather relax to another equilibrium configuration. Since the MSD in the z direction does not change drastically during these 1000 time steps while the MSD's in the x and y directions change substantially, we can say that the rearrangement of the molecular configuration takes place mainly in the layers. After this time, all three MSD's approach their respective constant values except for some small fluctuations. This indicates that the resulting equilibrium configuration is in a solid state.

In order to investigate this final configuration in detail, we first calculate the total pair-distribution function $g_\perp$ which is defined by the projected value of r_{ij} into the xy plane. The result is shown in Fig. 8 where $r_\perp$ is measured in units of the specific length $l_\perp = [L_\perp^2/(\text{number of molecules in a layer})]^{\frac{1}{2}}$, where $L_\perp$ is the edge length of the simulation box perpendicular to the molecular axis. Note that $l_\perp$ is nearly equal to the intermolecular distance a but is not identical with a since a triangular lattice is embedded in a square-shape cross section of a right parallelepiped simulation box. A strong correlation remains even for large values of $r_\perp/l_\perp$, indicating that the final configuration is the crystalline structure. Note that there is a peak also at $r_\perp = 0$, hereafter referred to as the zeroth peak, which reflects the fact that the same kind of layer, say A, appears more than once. The second peak at $r_\perp(\text{2nd})/l_\perp \simeq 1.08$ corresponds to the nearest-neighbor position of molecules in the same layers. The first peak at $r_\perp(\text{1st})/l_\perp \simeq 0.611$ is due to the approximate close-packed stacking between adjacent layers. The difference between the third-peak position $r_\perp(\text{3rd})/l_\perp \simeq 1.65$ and the first peak position is about 1.0, indicating that the first and third peaks are brought about by molecules in the same layer or in two different layers of the same type. Similarly, we can also show that the differences between the positions of the other odd peaks (third and fifth, fifth and seventh, and seventh and ninth) and between the even peaks (second and fourth, fourth and sixth, and sixth and eighth) are almost 1.1 for all these cases, which clearly suggests that the system is crystalline.

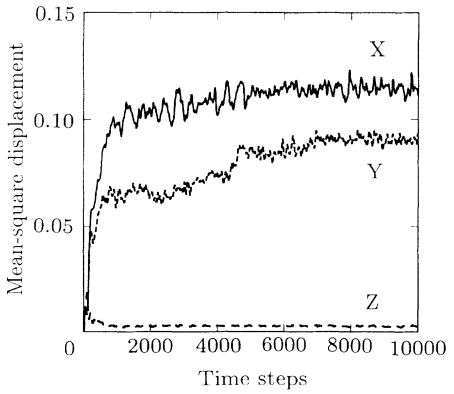

FIG. 7. Mean-square displacement of a system of N=600 soft parallel spherocylinders in the crystal region ($\rho^* = 0.534$). The solid curve denotes the diffusion in the x direction, the dashed curve in the y direction, and the broken curve denotes the diffusion in direction z which is parallel to the molecular axis.

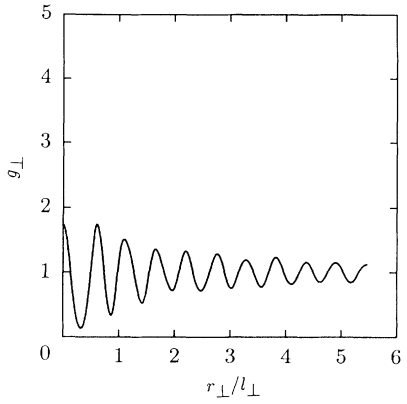

FIG. 8. Total pair-distribution function $g_\perp$ along the direction perpendicular to the molecular axis as a function of the distance $r_\perp/l_\perp$ at $\rho^* = 0.534$.

For the purpose of studying the molecular structure within a layer, we define that two molecules are in the same layer when $-L/2 \leq dz_{ij} \leq +L/2$, and then we calculate the in-layer pair-distribution function $g'_\perp$ as a function of $r_\perp/l_\perp$ for which the molecules only in the same layer are counted (Fig. 9). Figure 9 shows a clear crystalline structure of a two-dimensional close-packed (triangular) lattice. An exact triangular lattice consists of peaks $r_\perp/a = n$, $r_\perp/a = \sqrt{3}n$, and $r_\perp/a = \sqrt{n^2+3n+3}$, where $n = 1, 2, 3, \ldots$. Around each molecule there exist six molecules at the distance $r_\perp/a = n$ and at $\sqrt{3}n$, and 12 molecules at $r_\perp/a = \sqrt{n^2+3n+3}$. From the calculation of the average position of the first peak, we estimate $a \simeq 1.07 l_\perp$. The four

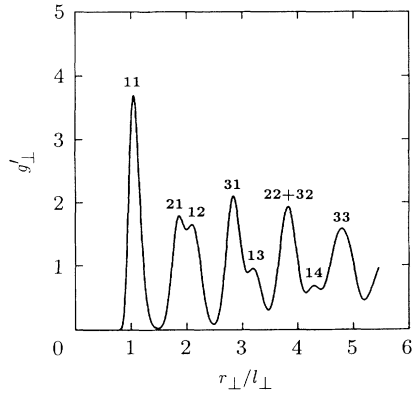

FIG. 9. Pair-distribution function $g'_\perp$ of molecules in the same layers vs $r_\perp/l_\perp$ at $\rho^* = 0.534$.

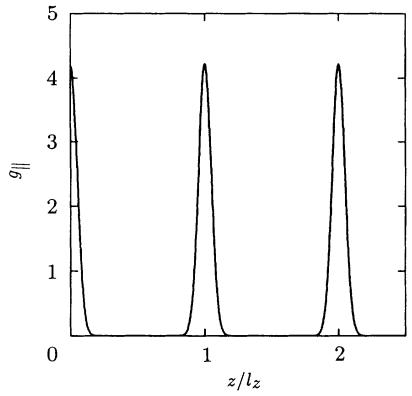

FIG. 10. Pair-distribution function $g_{\|}$ in the direction parallel to the molecular axis as a function of distance z/l_z at $\rho^* = 0.534$.

peaks denoted as peaks 11, 12, 13, and 14 in Fig. 9 are respectively located at $r_\perp/l_\perp \simeq 1.07$, 2.10, 3.20, and 4.29. Since $a \simeq 1.07 l_\perp$ as mentioned above, we have $r_\perp/a \simeq 1.00$, 1.96, 2.99, and 4.01. It is clear that these peaks correspond to the peaks at $r_\perp/a = n$ for $n = 1$, 2, 3, and 4. The position of peak 21 is $r_\perp/l_\perp \simeq 1.86$ or equivalently $r_\perp/a \simeq 1.74$ which corresponds to $r_\perp/a = \sqrt{3n}$ for $n = 1$. On the other hand, the peak 31 at $r_\perp/l_\perp \simeq 2.84$ (or $r_\perp/a \simeq 2.65$) corresponds to $r_\perp/a \simeq \sqrt{n^2+3n+3}$ for $n = 1$. This peak assignment makes clear the reason for the splittings of the second and third peaks. As for the fourth peak, there does not appear a splitting except for a small subpeak 14 at $r_\perp/l_\perp \simeq 4.29$. This is because two peaks 22 and 32 corresponding to the peaks at $r_\perp/a = \sqrt{3n}$ and at $\sqrt{n^2+3n+3}$ for $n = 2$ are close to each other. The peak denoted as 33 at $r_\perp/l_\perp \simeq 4.80$ in Fig. 9 corresponds to the peak $r_\perp/a = \sqrt{n^2+3n+3}$ for $n = 3$.

Figure 10 describes the pair distributions in the direction parallel to molecular axis $g_{\|}$ as a function of z/l_z. From this figure, together with the results shown in Figs. 8 and 9, we can now conclude without any doubt that the system has a periodic layer structure. This pair-distribution function shows that there exist five layers in this system.

Finally we take a look at the average position of each molecule projected into the plane perpendicular [Fig. 11(a)] and parallel [Fig. 11(b)] to the molecular axis. We can see from these projections that repeat layers, say AA, do not occur. These figures show that the final configuration has a stacking of $ABCAB$.

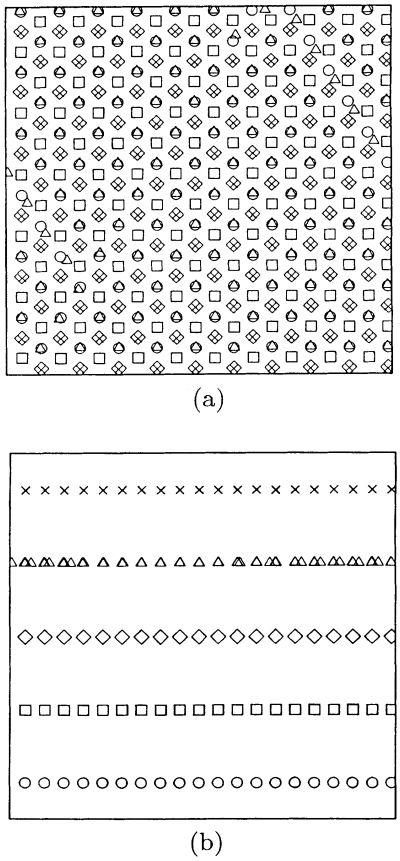

FIG. 11. Average positions projected into the plane (a) perpendicular and (b) parallel to the molecular axis at $\rho^* = 0.534$.

2. *Smectic-liquid-crystal phase*

Let us now study the low-density region below the transition. To be precise, the results in this section are for density $\rho^* = 0.416$. The results discussed are all for system size $N = 600$. In this case, the MSD's in Fig. 12 of each direction x, y, and z show a behavior significantly different to that for a crystalline-solid phase as shown in Fig. 7. After around 3000 time steps, the MSD's in the directions perpendicular to the molecular axis (solid curve, x direction; dashed curve, y direction) continue to increase while in the direction along the molecular axis (broken curve, z direction) it becomes almost constant.

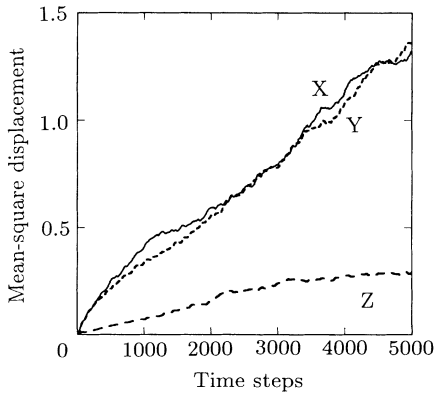

FIG. 12. Mean-square displacement of a system of N=600 soft parallel spherocylinders in the lower density phase ($\rho^* = 0.416$). The solid curve denotes the diffusion in the x direction, the dashed curve in the y direction, and the broken curve the z direction which is parallel to the molecular axis.

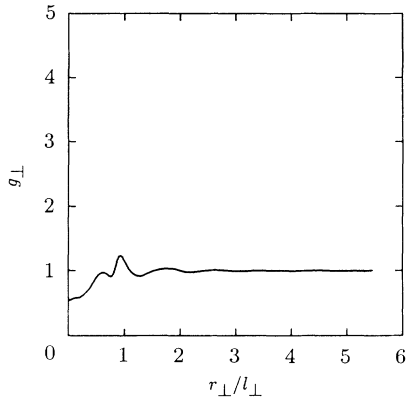

FIG. 13. Total pair-distribution function $g_\perp$ along the direction perpendicular to the molecular axis as a function of the distance $r_\perp/l_\perp$ at $\rho^* = 0.416$.

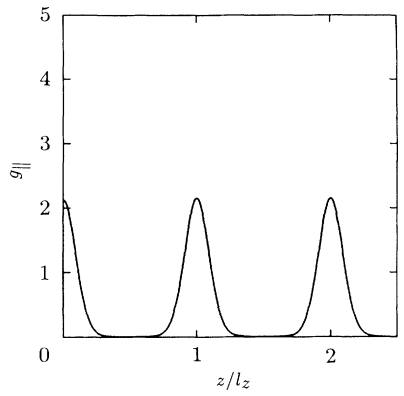

FIG. 15. Pair-distribution function $g_\parallel$ in the direction parallel to the molecular axis as a function of the distance z/l_z at $\rho^* = 0.416$.

From behavior of the MSD's in the x and y directions, we can see that diffusion takes place along the layer which is characteristic of the smectic-liquid-crystal phase.

Again, we calculate $g_\perp$ for this system as shown in Fig. 13, which is entirely different from $g_\perp$ for a crystal shown in Fig. 8. It must be noted that $l_\perp$ at this density is 7% less than $l_\perp$ in a crystal studied in the preceding Sec. III B 1. To begin with, there is a dip at $r_\perp/l_\perp = 0$ in this case as seen in Fig. 13 while there exists a sharp peak at $r_\perp/l_\perp = 0$ for a crystal as shown in Fig. 8. The dip at $r_\perp/l_\perp = 0$ in Fig. 13 indicates that, in this phase, there exists no correlation between the molecular configurations of two distant layers. This is not the case for a crystalline phase in which two distant layers can be of the same type, say A and A, which is the origin of the peak at $r_\perp/l_\perp = 0$ in Fig. 8. As for the first peak, there is a small hump at $r_\perp/l_\perp \simeq 0.626$ which indicates that the molecules are diffusing in a manner that the spherocylinders in adjacent layers are avoiding each other and percolating through the protuberance of the sphere caps, and yet there is a vestige of interlayer close pack remaining as observed in some real smectic-B phases [12]. The second peak at $r_\perp/l_\perp \simeq 0.925$ corresponds to the intermolecular distance in the layer. An interesting point to make here is that this distance is about 1 when measured by $l_\perp$ for a crystal. This means that the expansion of the system is not homogeneous. This total transverse pair-distribution function $g_\perp$ becomes structureless beyond the second peak.

The pair-distribution function $g'_\perp$ inside the layers (Fig. 14) for this smectic region ($\rho^* = 0.416$) shows a behavior typical of a liquid. When we compare Fig. 14

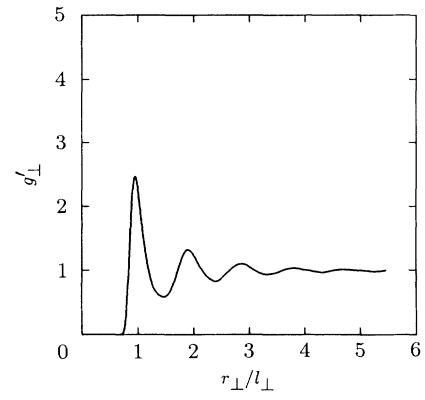

FIG. 14. Pair-distribution function $g'_\perp$ of molecules in the same layers vs $r_\perp/l_\perp$ at $\rho^* = 0.416$.

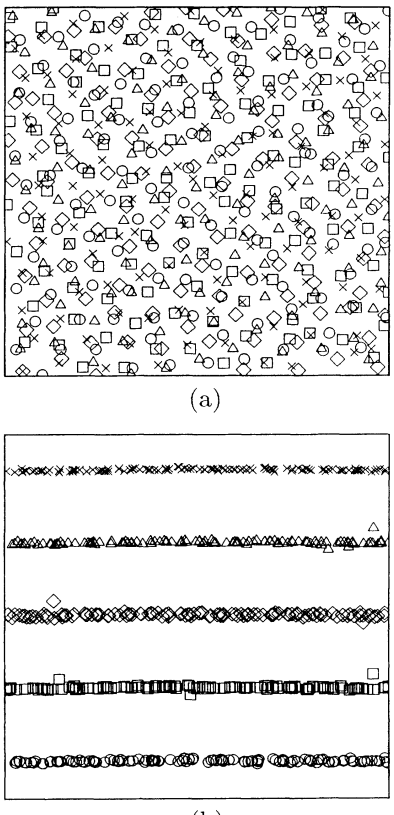

FIG. 16. Average position projected into a plane (a) perpendicular and (b) parallel to the alignment at $\rho^* = 0.416$.

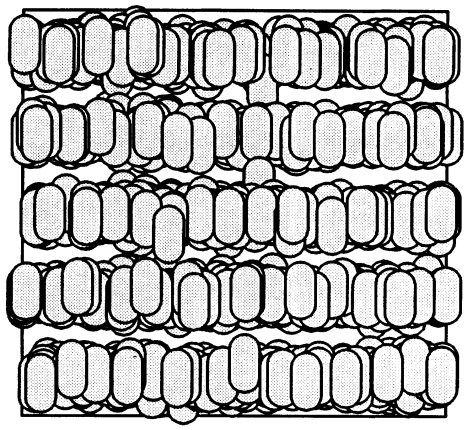

FIG. 17. Snapshot of $N = 600$ molecules at $\rho^* = 0.416$ from the direction perpendicular to the alignment.

with Fig. 13, we can see that the molecules in the same layer have a liquidlike correlation while those in different layers no longer show correlations.

The pair-distribution function $g_{\|}$ in the direction parallel to the molecular axis is shown in Fig. 15. Although the peak values are almost half and the peaks are wider compared to the crystalline-solid phase, $g_{\|}$ still shows a strong periodic density oscillation. This is firm evidence of the layer structure characteristic of the smectic phase.

We check the average positions of the molecules by projecting them into a plane perpendicular [Fig. 16(a)] and parallel [Fig. 16(b)] to the molecular axis. From the latter figure, we can see clear layers while the former figure confirms the liquidlike structure in each layer.

Finally Fig. 17 shows a snapshot of the system with $N = 600$ molecules. A layer structure with a small fluctuation of the molecular positions is observed.

IV. CONCLUDING REMARKS

In this paper, we have presented results of constant-pressure MD simulations for systems of soft parallel spherocylinders. Conventional simulation methods are not appropriate for treating anisotropic molecules since they do not always give isotropic hydrostatic pressure. We have tried several different methods of constant-pressure MD simulations in order to reveal the nature of the transition from crystalline solid to smectic liquid crystal. We find that it is necessary to vary the shape of the MD simulation box when simulating anisotropic molecules. Thermodynamic properties and structural analysis show that a clear first-order crystal-smectic transition occurs in such systems. In the crystalline-solid phase, the spherocylinders are stacked in a close-packed manner and do not diffuse after reaching equilibrium. In the smectic phase, the MSD's and the pair-distribution functions show that the molecules in a layer diffuse in a manner that retains some vestiges of the packed stacking of adjacent layers. By observing the molecular length parallel l_z and perpendicular $l_{\perp}$ to the molecular long axis at the transition, we find that the molecules melt along the layers and that the anisotropy of the molecular volume (the ratio $l_z/l_{\perp}$) plays a very important role.

ACKNOWLEDGMENTS

Authors are grateful to Sumitomo Chemicals for supplying computational time. We would also like to thank Dr. S. Nosé and Dr. S. Sakamoto for valuable discussions.

[1] S. Chandrasekhar, Contemp. Phys. **29**, 527 (1988).
[2] L. Onsager, Ann. N.Y. Acad. Sci. **51**, 627 (1949).
[3] M. Hosino, H. Nakano, and H. Kimura, J. Phys. Soc. Jpn. **46**, 1709 (1979); **47**, 740 (1979); **51**, 741 (1982).
[4] B. J. Alder and T. E. Wainwright, J. Chem. Phys. **27**, 1208 (1957).
[5] D. W. Rebertus and K. M. Sando, J. Chem. Phys. **67**, 2585 (1977).
[6] A. Stroobants, H. N. W. Lekkerkerker, and D. Frenkel, Phys. Rev. A **36**, 2929 (1987).
[7] J. A. C. Veerman and D. Frenkel, Phys. Rev. A **41**, 3237 (1990).
[8] W. G. Hoover, S. G. Gray, and K. W. Johnson, J. Chem. Phys. **55**, 1128 (1971).
[9] H. C. Andersen, J. Chem. Phys. **72**, 2384 (1980).
[10] M. Parrinello and A. Rahman, Phys. Rev. Lett. **45**, 1196 (1980).
[11] S. Nosé and M. L. Klein, Mol. Phys. **50**, 1055 (1983).
[12] A. J. Leadbetter, J. C. Frost, and M. A. Mazid, J. Phys. (Paris), Lett. **40**, 325 (1979).

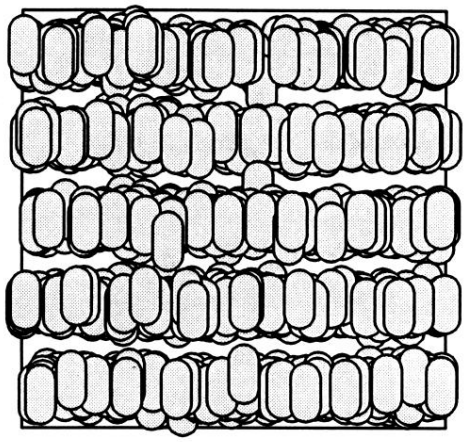

FIG. 17. Snapshot of $N = 600$ molecules at $\rho^* = 0.416$ from the direction perpendicular to the alignment.